



Experimental and DFT insights into optical and magnetic studies of graphene oxide/ZnFe₂O₄ nanocomposites for enhanced photodegradation

G. Nandhini¹ · D. Vignesh² · M. K. Shobana¹ · S. Kavita³ · T. Pazhanivel⁴

Received: 3 January 2024 / Accepted: 30 March 2024 / Published online: 9 April 2024
© King Abdulaziz City for Science and Technology 2024

Abstract

Functional nanoferrites are attracting interest in photocatalytic applications due to their intriguing and excellent optical and magnetic properties. In that order, as suitable adsorbents for wastewater treatment, graphene-based nanoferrites can be tuned. In this article, ZnFe₂O₄/GO nanocomposites have been prepared to study the structural, optical, magnetic, and photocatalytic properties through investigational (experimental) results and theoretical insights. Further, the synthesized nanocomposites fall under the mesoporous range with an average crystalline size of around 15–18 nm with good colloidal stability. Spherically agglomerated morphology has been observed by FE-SEM analysis. Magnetic characterizations were done by vibrating sample magnetometer (VSM) with superparamagnetic behavior at room temperature (RT). Optical insights reveal that the samples exhibit good photocatalytic properties with a degradation rate of 85.8% with methylene blue (MB) organic pollutant. Hence, this article aims to study the properties of prepared ZnFe₂O₄/GO nanocomposites through a detailed theoretical discussion of density functional theory (DFT).

Keywords Zinc ferrite · Density functional theory · Dye degradation · Methylene blue · Graphene oxide

Introduction

The global problem of waste-water contamination and its treatment has been made worse by the world's population's rapid rise as well as the tremendous development of industry and technology. As of now, the many different types of dyes that pollute surface and groundwater constitute harm to both humans and aquatic life. The carcinogenic and mutagenic

properties of dyes make them one of the most hazardous organic pollutants (Bhuvaneswari et al. 2021). Textile dyes are a hazardous contaminant for aquatic ecosystems because, in several cases, the molecules of dye are impervious to the method of handling employed in treating wastewater as a result of their minimal degradation and complicated structure. Worldwide, many methods of scavenging them have been developed and employed. Magnetic separation techniques have been employed in various fields, including water treatment, as a fast and effective approach (Fei et al. 2016).

In addition to their high pH, chemical and biochemical oxygen demand, and salts, the effluents produced by the dyeing and textile sectors include blends of metals, dyes, and other contaminants. Without rehabilitation, the accidental discharge of these materials into aquatic spaces will result in several environmental issues. For example, dyes alter the optical appeal of water bodies and block light from penetrating the water's surface, which slows down photosynthesis and lowers the supply of oxygen required by aquatic life. It is concerning that persistent pollutants exist in aquatic environments because they easily penetrate or pierce aquatic species and spread to other organisms via the cycles of the food chain (Ahmed et al. 2022).

✉ M. K. Shobana
mkshobana@gmail.com

¹ Department of Physics, School of Advanced Sciences, Vellore Institute of Technology, Vellore, Tamil Nadu 632014, India
² Birla Institute of Technology, Mesra, Ranchi, Jharkhand 835215, India
³ Centre for Automotive Energy Materials, International Advanced Research Centre for Powder Metallurgy and New Materials (ARCI), IIT-M Research Park, Chennai, Tamil Nadu 600113, India
⁴ Smart Materials Interface Laboratory, Department of Physics, Periyar University, Salem, Tamil Nadu 636011, India

Organic contamination due to decomposition via photocatalytic processes is one of the significant and prospective environmentally friendly chemical methods. Additionally, the use and requirement of photo-catalysts today might be beneficial in tracking environmental pollutants. Researchers found a major issue with the beneficial application of photocatalyst therapy in wastewater treatment (Sudha and Sivakumar 2015). It is expensive, laborious, and difficult to separate the photocatalyst substance from the effluent. The most significant benefit of implementing nanoparticles with magnetic properties in photocatalysis has the ability to be separated after the reaction concludes by means of an external magnetic field. Due to its outstanding magnetic properties, ease of magnetic separation of solids after adsorption, high adsorption capacity and surface area, iron oxide nanoparticles have captured the interest among researchers (Sutka et al. 2015). They are also specifically successful in removing a broad spectrum of pollutants that are both organic and inorganic.

ZnFe₂O₄ has received a lot of investigation in the photochemical synthesis of hydrogen from water and its transformation of solar energy. Additionally, the magnetic ZnFe₂O₄ particles had intrinsic peroxidase-like activity that might interact with hydrogen peroxide (H₂O₂) to create ·OH ions. Zinc ferrite nano catalysts can be reactivated up several times substantially without losing their catalytic activity due to their magnetic characteristics (Ajormal et al. 2020). Electron–hole pair reintegration is typically delayed or prevented by photon-excited particles in tiny clusters because photon-generated e[−] and h⁺ pairs typically take 9 to 10 s to recombine.

Additionally, several carbon-based compounds have been employed as adsorption agents in purifying wastewater (Qadir et al. 2021). In fact, activated carbon materials, which have been extensively used in the pigmented wastewater treatment sector, that have a significant adsorption capability due to their extensive pores and huge surface area. A novel, burgeoning carbon-based substance called graphene oxide (GO) is widely recognised as a promising adsorbent in the elimination of pigment molecules from water, as GO has exceptional adsorption characteristics (Pham et al. 2022).

Mahmood et al. prepared spinel ferrite nanostructures at the surface of reduced graphene oxide sheets through a facile chemical route. The main incorporation of graphene was to enhance the conductivity of the ferrite particles with the utilization of methylene blue dye (Mahmood et al. 2018). Similarly, the use of reduced graphene oxide with pure zinc ferrite nanoparticles for the degradation of methylene blue dye exhibits the significant role of hydroxyl radicals in the scavenger test with the degradation of around 92% after three cycles (Baynosa et al. 2020). Further, Farhang et al., synthesized zinc ferrite nanoparticles with graphitic carbon nitride (g-C₃N₄) and showed an efficiency of about 98% for

methylene blue dye degradation facilitating the transfer of electrons by incorporating graphene particles (Farhang et al. 2024). Bibi et al. synthesized zinc ferrites by incorporating transition metals like Ni and Mn co-doped zinc ferrites through the co-precipitation method with 10% addition of rGO. The study exhibits a degradation rate of about 94.6% for malachite green (MG) dye (Bibi et al. 2024). Still, several studies undergo photocatalytic reactions with the incorporation of graphene oxide/reduced graphene oxide with different preparation techniques (Sonu et al. 2023; Patial et al. 2022; Nandhini et al. 2023; Parasuraman et al. 2023). Thus, different preparation techniques have an impact on the overall structure, size, and morphology, all may influence the photocatalytic function.

The synthesis of magnetic ferrite and ferrite-GO nanocomposite adsorption agents with high saturated magnetization allows for an outstanding magnetic separation of the adsorption material, which is a crucial technology for its broad usage in the waste water management space (Liu et al. 2012). Therefore, this work significantly elucidates the experimental and theoretical (DFT) correlation between the structural, magnetic, and photocatalytic properties of pure ZnFe₂O₄ and ZnFe₂O₄: GO nanocomposites through MB organic pollutant.

Materials and method

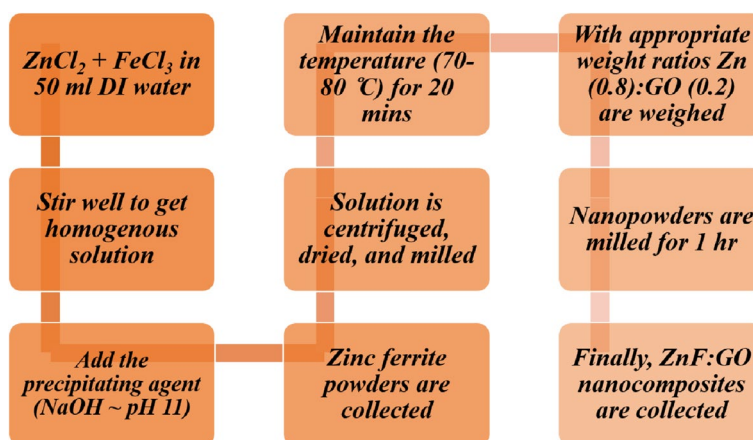
Experimental details

ZnFe₂O₄ with graphene oxide nanocomposites with weight ratios were synthesized by chemical co-precipitation (Latif et al. 2023) and solid-state reaction technique. Initially, ZnFe₂O₄ nanoparticles with accurate stoichiometric amounts were dissolved in milli Q-water along with the addition of NaOH (1 M) as a precipitating agent. The solution was heated upto 80 °C and cooled to room temperature. Further, the solution went under centrifugation, drying, and annealing. The annealed sample was milled for 30 min to form zinc ferrite nanoparticles. On the other side, graphene oxide was prepared by the modified hummers method (Chen et al. 2013). Finally, with appropriate weight ratios, zinc ferrite, and graphene oxide powders were milled for 2 h to get the ZnFe₂O₄/GO nanocomposites and labeled as ZnF (pure ZnFe₂O₄) nanoparticles and ZnF-GO (ZnFe₂O₄/GO) nanocomposites, respectively. A detailed experimental process is illustrated in Fig. 1.

Computational details

Pure and GO-doped ZFO structures were geometrically optimized with 500 eV plane wave cut-off and 2 × 3 × 3 k-mesh and Gaussian smearing with a constant smearing width of

Fig. 1 Experimental illustration of pure ZnFe_2O_4 and ZnF:GO nanocomposites



0.05 in DFT- VASP simulation software. A constant energy difference of 1×10^{-6} eV was preserved between successive self-consistent iterations. The relativistic effects namely the spin polarization were incorporated via a semiempirical DFT + U approach according to Dudarev et al. (Dudarev and Botton 1998) with $U_{\text{eff}} = 5$ eV for all material constituents. The electronic parameters (Band structure and density of states) were evaluated under Tetrahedral smearing. The magnetic response of the dual compositions was recorded under the influence of spin polarization effects.

Characterization

The structural properties of the samples were determined using the X-ray diffractometer (Bruker D8 Advance with $\text{Cu-K}\alpha$ radiation). Functional group elements were identified by FTIR (Shimadzu IRAffinity-1). Morphology was confirmed by FE-SEM (Carl Zeiss Sigma 300). Sample's colloidal stability is observed by zeta potential analysis using Litesizer 500, Anton Paar GmbH, Austria. Magnetic measurements were performed at both room (RT) and low temperatures (LT) using vibrating sample magnetometer by Quantum Design, Dynacool-9 T. Further, optical and photocatalytic properties were studied by UV spectrophotometer (Jasco-UV-Visible spectrophotometer (V-670 PC)).

Results and discussion

X-ray diffraction

Figure 2b, c shows the X-ray diffraction patterns of graphene oxide (GO), zinc ferrite (ZnFe_2O_4), and ZnFe_2O_4 :GO nanocomposites. Pure and graphene oxide (GO) doped ZnFe_2O_4 (ZFO) are some of the typically biocompatible spinel ferrites with a cubic fcc core and AFe_2O_4 periodic formula unit. The conventional example of an antiferromagnetic normal spinel ferrite is bulk ZnFe_2O_4 , but the nanostructures change the

cationic ordering to form ferrimagnetic mixed spinel structures with ($0 < x < 1$) as the general formula for partial tetrahedral and octahedral occupancy (Ait Kerroum et al. 2019). The Zn-O_4 tetrahedrons are interlinked with the octahedral interstices via 3-D percolation channels within the 8 formula units of ZFO respectively. However, a synergetic 72 vacant interstices due to 16 vacant octahedral and 56 vacant tetrahedral sites within $\text{Zn}_8\text{Fe}_{16}\text{O}_{32}$ allows the transfer of cations within the unit cell and hence the resultant cationic rearrangements (Szotek et al. 2006).

All the diffraction peaks of the hybrid nanocomposite can be assigned to the cubic spinel phase of ZnFe_2O_4 (JCPDS: 89-7412) (Guo et al. 2014). The characteristic peaks observed are attributed to the crystal planes of (111), (220), (311), (400), (422), (511), and (440) from the cubic system of zinc ferrite. Furthermore, the strong intensity diffraction peaks suggest that both the ZnFe_2O_4 and ZnFe_2O_4 :GO nanocomposites are well crystallized. The essential parameters like crystalline size, lattice constant, interplanar spacing, unit cell volume, and hopping length are calculated by the equations given in our previous work (Shobana et al. 2022). The atomic ordering, chemical composition of pure, and doped composition sets the foundation for biochemical attributes. Figure 2a illustrates the DFT simulated X-ray diffractogram of host and GO doped spinel ferrite.

The simulated XRD profile of host and GO-doped compositions with intense peaks over $2\theta = 10-90^\circ$ display polycrystalline mixed spinel structure with $Fd\bar{3}m$ cubic symmetry devoid of impurity phase. The prominent peak corresponding to (311) affirms the characteristic spinel structures of dual compositions that agrees with our experimental assessment as shown in Fig. 2b, c respectively. The magnetic nature (ferromagnetic/ferrimagnetic/superparamagnetic/antiferromagnetic) of the resultant ZFO-based spinel nano ferrites rely upon the A and B cationic ordering alongside the strength of A–A and B–B ionic bonds with $\text{A}^{2+}\text{–O–B}^{3+}$ super-exchange interactions (Dippong et al. 2021). However, the degree of the magnetic response of spinel nano ferrites

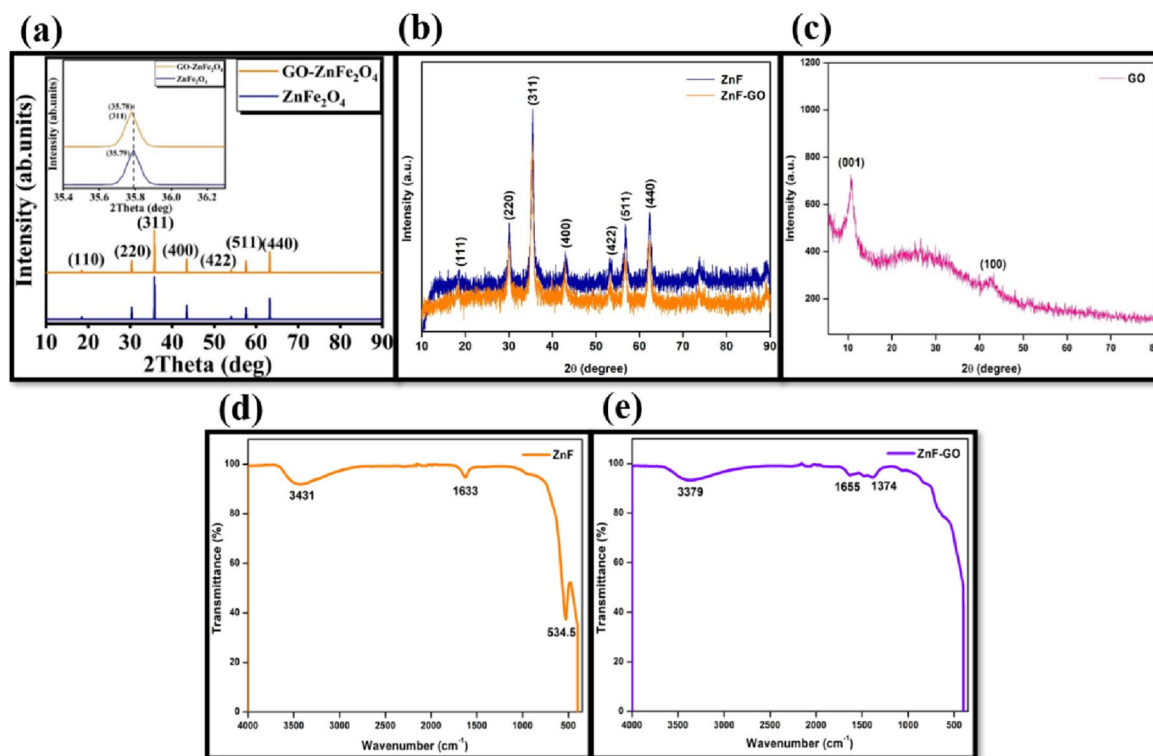


Fig. 2 **a** DFT simulated XRD profile of ZnFe_2O_4 and GO-doped ZnFe_2O_4 (inset: magnified section of (311) indicating peak shifts), **b** graphical illustration of graphene oxide (GO), **c** XRD pattern of

ZnFe_2O_4 (ZnF) and ZnFe_2O_4 : GO (ZnF-GO) nanocomposites, **d** FTIR for ZnFe_2O_4 nanoparticles, and **e** FTIR for ZnFe_2O_4 /GO nanocomposites

is mediated by the oxygen anions and relies upon the A–B interactions over their symmetric counterparts (Fesenko et al. 2017). As a result, the magnetic dipolar separation within ZFO and GO-doped ZFO mixed spinel nano ferrites occur due to Zn^{2+} – Fe^{3+} and Fe^{2+} – O – Fe^{3+} interactions with the host binary oxide.

According to the experimental analysis, the incorporation of graphene oxide with ZnFe_2O_4 nanoparticles results in an increased average crystalline size from 15.64 to 18.13 nm. The lattice parameters can be calculated using the values of d-spacing, which were calculated by the Bragg law and compared to the values reported in the JCPDS card. As the lattice parameters and crystalline size depend on each other, it increases with an increase in crystalline size and decreases with the breakdown of material bonds (Garza-Tovar et al. 2006). Also, the strain formed by the substitution in the cell makes the crystalline size to increase. Thus, the lattice parameters and the average crystalline size of the nanoparticle would depend on the ionic radii and the temperature variations of the material. With the increase in lattice parameters, unit cell volume also increases.

In the XRD patterns of the ZnF-GO, (001) usually does not appear due to the diffraction peaks of nanocrystals of Zn being much stronger than the (001) of GO and also may be attributed to the removal of oxygen-containing groups of

GO. It is the reason for the increase in interplanar spacing of the ZnFe_2O_4 : GO nanocomposites. Further, the appropriate distance between the tetrahedral (L_A) and octahedral sites (L_B) of magnetic ions is termed hopping length, which plays a significant role in determining the physical properties of the ferrites. The slight increase in hopping length is due to the distance between the magnetic ions increasing with the incorporation of the GO. Consequently, the results show that the increase in lattice constant is primarily due to the observance of a slight blue shift. Further, the bond length and shared and unshared edges of tetrahedral and octahedral sites are revealed in Tables 1 and 2 and are calculated from the Eq. (1–5) (Patil et al. 2021) below,

$$d_{AX} = a\sqrt{3}\left[u - \left(\frac{1}{4}\right)\right]\text{\AA} \quad (1)$$

$$d_{BX} = a\left[3u^2 - \left(\frac{11}{4}\right)u + \left(\frac{43}{64}\right)\right]^{1/2}\text{\AA} \quad (2)$$

$$d_{AXE} = a\sqrt{2}\left[2u - \left(\frac{1}{2}\right)\right]\text{\AA} \quad (3)$$

$$d_{BXE} = a\sqrt{2}(1 - 2u)\text{\AA} \quad (4)$$

Table 1 XRD parameters of graphitic zinc ferrite nanocomposite

Sample name	Crystalline size (D) (nm)	Lattice constant (a) (Å)	Interplanar spacing (d) (Å)	Unit cell volume (V) (Å ³)	L _A (Å)	L _B (Å)
ZnF	15.64	8.411	2.071	595.07	3.642	2.973
ZnF–GO	18.13	8.416	2.594	596.12	3.644	2.975

Table 2 Determination of some parameters like tetrahedral bond length (d_{AX}), octahedral bond length (d_{BX}), tetrahedral edge (d_{AXE}), shared octahedral edge (d_{BXE}), and unshared octahedral edge (d_{BXEU})

Sample name	d _{AX} (Å)	d _{BX} (Å)	d _{AXE} (Å)	d _{BXE} (Å)	d _{BXEU} (Å)
ZnF	1.908	2.048	3.115	2.830	2.967
ZnF–GO	1.909	2.050	3.117	2.832	2.969

$$d_{\text{BXEU}} = a \left[4u^2 - 3u + \left(\frac{11}{16} \right) \right]^{(1/2)} \text{Å} \tag{5}$$

From the theoretical investigation, the XRD profile of GO-doped ZFO displays the absence of its characteristic peaks corresponding to 001 and 100 while, on the contrary, illustrating close congruence with the host composition, respectively. The consequent response is the outcome of the strong crystalline characteristic of the host composition with intense peaks. While structural invariance was preserved post GO substitution to the host composition, a marginal peak shift towards a lower angle observed indicating lattice expansion as shown in Fig. 2a. A subsequent rise in the simulated lattice parameter with GO substitutions is the outcome of cationic migrations between different interstices that also agrees with our experimental estimations. Table 3 represents the simulated geometrical parameters of the host and GO-doped compositions. Further, the lattice strain due to GO substitutions induces energy difference between two various interstices. Such energy landscape is responsible for several physiochemical behaviour of the resultant composition.

FTIR

The absorbance between pure ZnFe₂O₄ and graphene oxide/ZnFe₂O₄ nanocomposites is depicted in Fig. 2d, e. Table 4

displays the group of functional elements produced by each absorption. The Fe–O stretching vibrations at the tetrahedral site are represented by an absorbent signal with wave number of 530 cm⁻¹ in the FTIR spectrum (Sari and Hakim 2019). On the other hand, the Fe–O vibration is not seen in the ZnFe₂O₄/GO sample. Instead, a Zn–O–Fe stretching vibration that corresponds to the production of nanoferrites is observed around 1370 cm⁻¹. Additionally, the O–H stretching vibrations in the synthesised nanocomposites are indicated by a wavenumber around 3400 cm⁻¹ (Ali et al. 2022).

FE-SEM

Figures 3c, f depicts EDS spectra and micrographs with resolutions ranging from 100 nm to 1 μm. Pure zinc ferrite nanoparticles show spherical shape in clusters in their micrographs. As a result, zinc ferrite doped graphene oxide has an uneven form and aggregation. Pure ZnF particles surface morphology appears to be uniform in arrangement. All FE-SEM images demonstrate that they were extremely tiny with a high propensity to aggregate. The majority of chemically produced nanopowders exhibit high levels of agglomeration, which is probably a consequence of tiny fundamental particles that have a

Table 4 Vibrational modes present in the prepared nanocomposite material

Functional group	Wave number (cm ⁻¹)		Vibrational mode
	ZnFe ₂ O ₄	ZnFe ₂ O ₄ /GO	
Zn–O (tetrahedral)	534.5	–	Stretching
Zn–O–Fe	–	1374	Stretching
H–O–H	1633	1655	Bending
O–H	3431	3379	H-bonded stretching

Table 3 DFT simulated lattice parameter of pure and GO-doped ZFO compositions

Composition	DFT simulated lattice parameter			Prior experimental evidence	% Error of DFT simulated parameters with respect to prior experimental report	Refs
	a (Å)	b (Å)	c (Å)			
ZFO	8.410	8.410	8.410	8.411	0.011	Pham et al. (2022)
GO–ZFO	8.414	8.414	8.414	–	–	

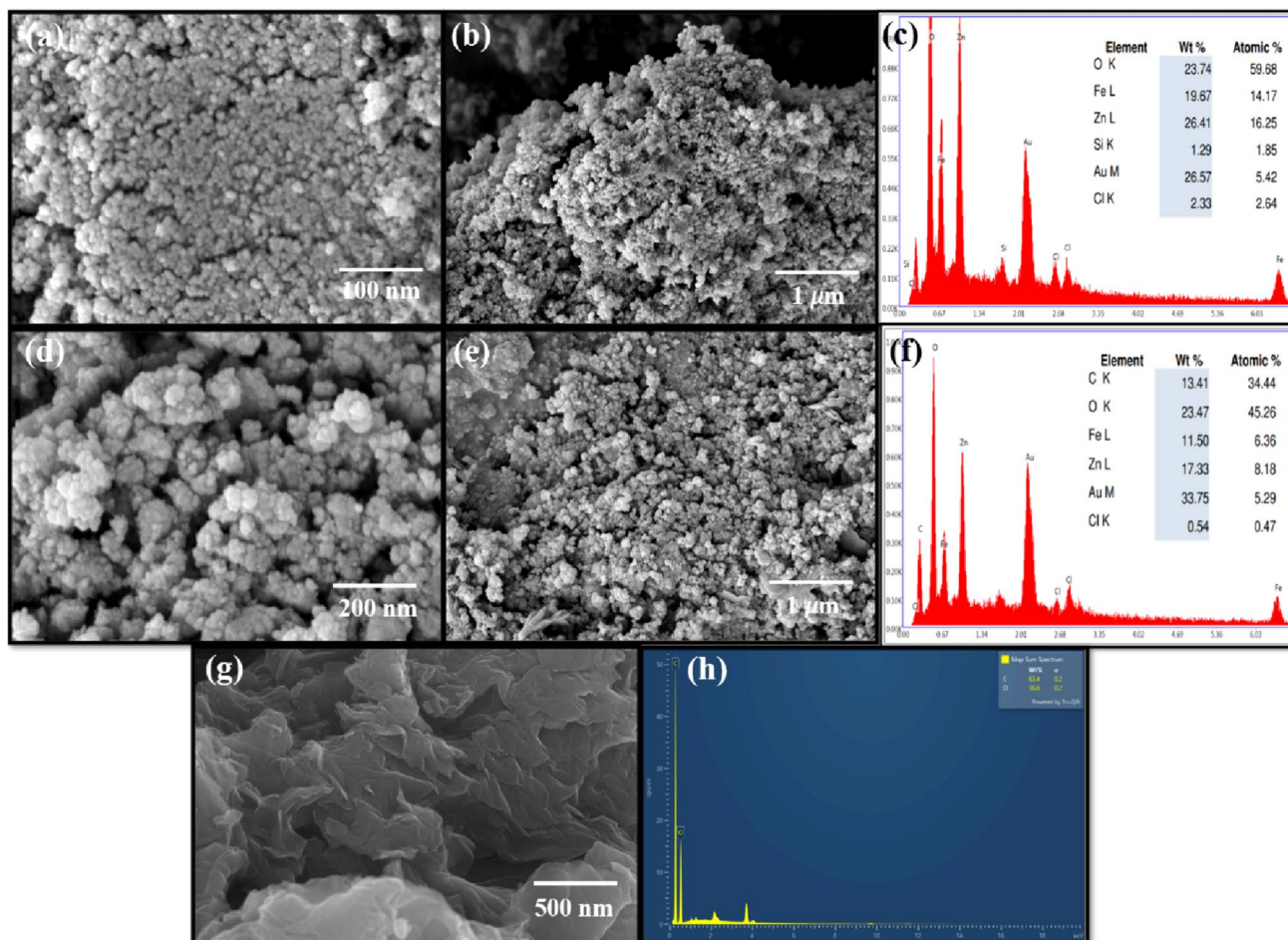


Fig. 3 FE-SEM images of **a, b** ZnF@100 nm and 1 μm, **c** EDS spectra and micrographs of ZnF NPs, **d, e** FE-SEM images of ZnF/GO@200 nm and 1 μm, **f** EDS spectra and micrographs of ZnF/GO

nanocomposites, **g** FESEM image of graphene oxide@500 nm and **h** EDS spectra and micrograph of ZnF/GO nanocomposites

propensity to clump together (Andjelković et al. 2018; Fei et al. 2023). As a result, it proves that ZnFe₂O₄ nanoparticles are evenly dispersed across the graphene oxide surface.

Furthermore, the list of substances existing in the produced nanocomposites is revealed by EDS spectra (Fig. 3c, f) (Džunuzović et al. 2015). The presence of Au is highlighted because the nanocomposites have been encased in gold (Au) to promote better morphology. Existence of precursor materials such as Cl is due to improper removal during centrifugation process. Si is noted as an impurity as well. However, the inclusion of graphene oxide to the zinc ferrite material results in the observation of carbon in the ZnF/GO material. Additionally, Si contamination is not observed in ZnF/GO composites. The spectra also display the atomic and weight ratios of the related compounds.

UV-Vis-NIR

Figure 4 shows the band gap values for the synthesised nanocomposites (ZnFe₂O₄ and ZnFe₂O₄/GO). The material's optical features can be studied using the UV spectra, which were recorded at room temperature. Utilising the same formula as in our previous study, the optical band gap energy was calculated (Shobana et al. 2022). The band gap values are derived from the reflectance spectrum by extrapolating the curves between the plane of the x-axis and $(\alpha h\nu)^2$ at the plane of the y-axis. With an increase in crystalline size values observed by XRD, the band gap values are decreased by adding graphene oxide to zinc ferrite. The best approach for a photocatalytic investigation would be a decreasing band gap energy with increased crystalline size. To confirm the above statement, theoretical investigation was also interpreted. Figure 5 demonstrates the

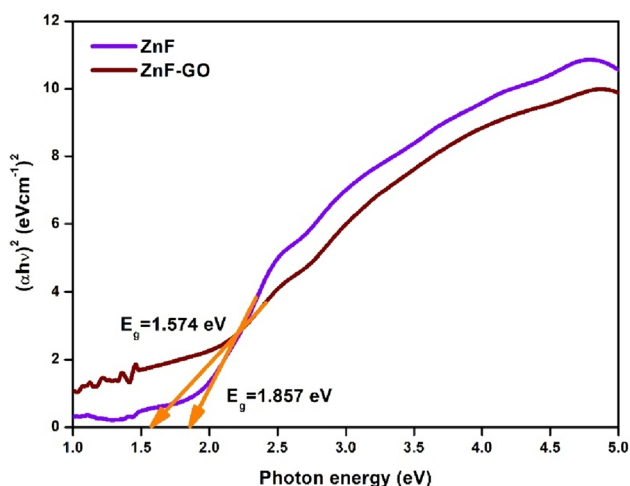
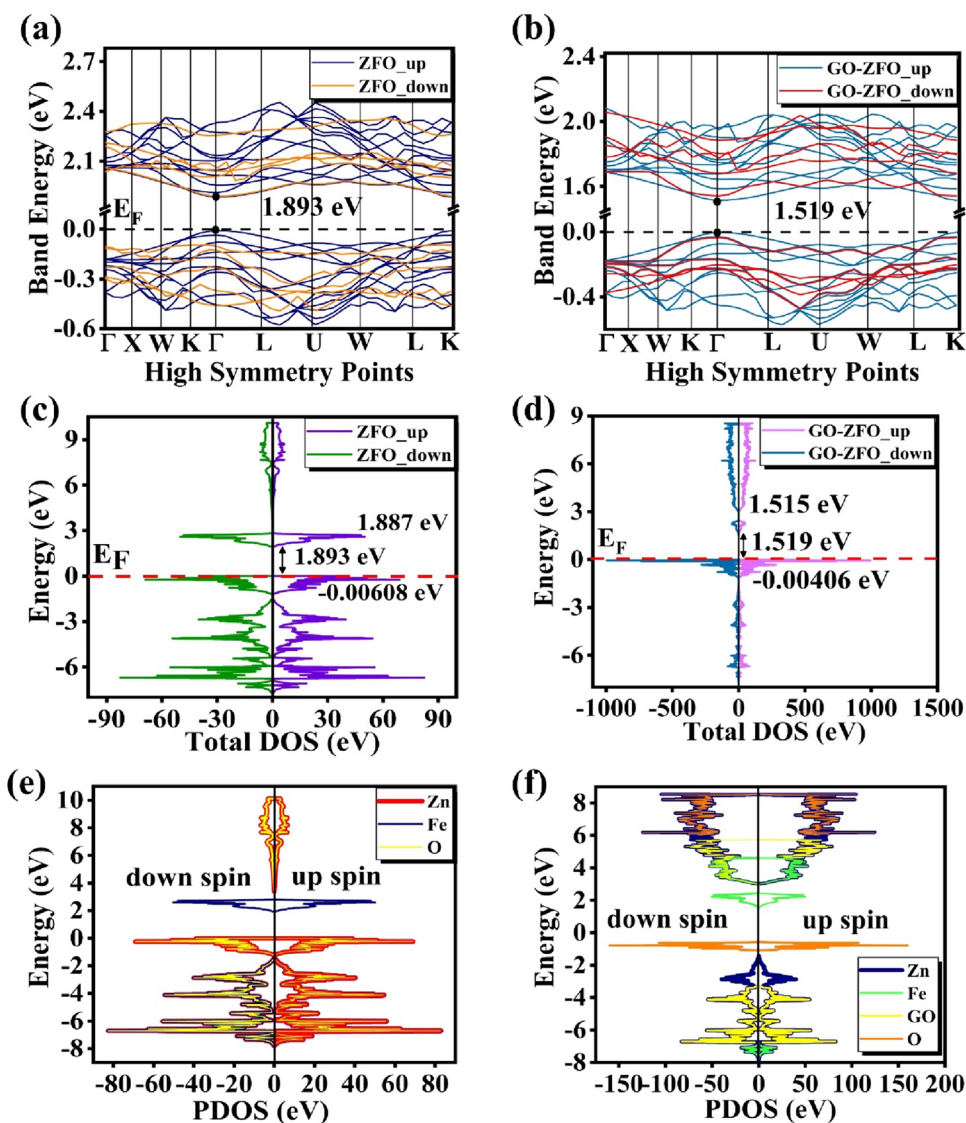


Fig. 4 Bandgap values of pure zinc ferrite and GO-doped zinc ferrite nanocomposites

band structure and density of states (DOS) of host and GO-doped ZFO compositions.

The DFT simulated electronic bandgap of ZFO spinel nano ferrites (1.893 eV) from Fig. 5b agrees with the experimental evidence (1.90 eV) of (Vinosha et al. 2017) followed by a decrease in the bandgap of GO-doped compositions due to a relative shift of GO and O-2p orbitals from the deep valance band towards the Fermi level (E_F). The band structure of principal ZFO comprises of O-2p with Fe -3d orbitals in the valance and conduction band respectively. While Fe-3d displays sufficient contributions in the conduction band top and deep valance band with the O-2p orbitals, Zn-3d on the contrary imparts fractional contributions to the conduction band. Hence, the observed and calculated band gap energy values for the prepared $ZnFe_2O_4$ and $ZnFe_2O_4/GO$ nanocomposites are almost identical.

Fig. 5 Electrophysical estimations of pure and GO-doped ZFO, **a** bandstructure of ZFO, **b** bandstructure of GO-doped ZFO, **c** total DOS of ZFO, **d** total DOS of GO-doped ZFO, **e** partial DOS of ZFO, **f** partial DOS of GO-doped ZFO



Zeta potential analysis

The dispersion of ZnFe_2O_4 NPs raises the zeta potential values (Fig. 6) are associated with decreased flocculation tendency. Due to the electrostatic attraction or repulsion between individual particles, a large negative value of zeta potential implies good stability of the nanosuspensions (Gaur et al. 2022). In water systems, the boundary value controlling the dispersion stability is believed to be approximately ± 30 mV (Kmita et al. 2019). The discovered Zeta potential value of -26.6 mV in the instance under examination ensures that the dispersion of zinc ferrite-incorporated graphene oxide nanocomposites would remain stable due to electrostatic repulsion. After several months of storage, a very small quantity of sedimentation was found in bottles of nanocomposites, proving that the dispersion of $\text{ZnFe}_2\text{O}_4/\text{GO}$ nanocomposites in water is stable. Consequently, the increase in Zeta potential values also increases the electrophoretic mobility of the particles in water from -0.000173 to -0.000205 cm^2/Vs for ZnFe_2O_4 and $\text{ZnFe}_2\text{O}_4/\text{GO}$ NCs, respectively (Table 5).

Magnetic analysis

Among diverse material properties, the magnetic response of spinel nanoferrites is extensively investigated for wastewater treatment applications. Spinel nanoferrites can be easily magnetized via structural variations and metallic substitutions where the magnetic property heavily relies upon the cationic ordering within the host lattice and the resultant crystal symmetry. The ease of magnetization of spinel structures emerges due to low magnetic anisotropy energy (Jalili et al. 2022). The genesis of magnetic behavior in spinel nanoferrites is strongly associated with the electronic structure and the hybridization of different material constituents.

Table 5 Zeta potential and electrophoretic mobility values for ZnF and ZnF/GO particles

Sample name	Zeta potential (mean) (mV)	Electrophoretic mobility (mean) (cm^2/Vs)
ZnF	-22.2	-0.000173
ZnF:GO	-26.4	-0.000205

The linear magnetization and low coercivity demonstrates the superparamagnetic nature of the zinc ferrite nanoparticles. Additionally, the samples are not saturated at 80 kOe, which suggests the presence of single domain and superparamagnetic particles. Figure 7 demonstrates that the M-H loops of the $\text{ZnFe}_2\text{O}_4/\text{GO}$ nanocomposites were not able to be saturated by the maximum field of 100 kOe (Rachna and Singh 2018; Hangai et al. 2017). It is a sign that the material has significant anisotropy. The M-H loops observed in the current study demonstrate a transition from a normal to a mixed spinel type with paramagnetic ordering in the cation distribution.

At a maximum field of 100 kOe at 300 K, the nanoscale ZnF nanoparticles display non-hysteresis magnetization. Superparamagnetic ZFO nanoparticles typically behave in a non-saturated stretched S-type magnetization with zero coercivity. Zero-field and field cooled (ZFC–FC) protocols are depicted in Fig. 8. With a temperature reduction from 400 K at 100 Oe, ZnF and ZnF/GO nanoparticle magnetization rises (Grasset et al. 2002; Gharagozlou and Bayati 2015). At a significantly higher temperature, both ZFC and FC magnetizations share a single curve that separates into separate curves at 165 and 248 K (T_s), respectively. It proves superparamagnetism, which shows the particles behave as separate, non-interacting magnetic nanoparticles with uniaxial anisotropy. The particles are blocked at 35 and 7 K for

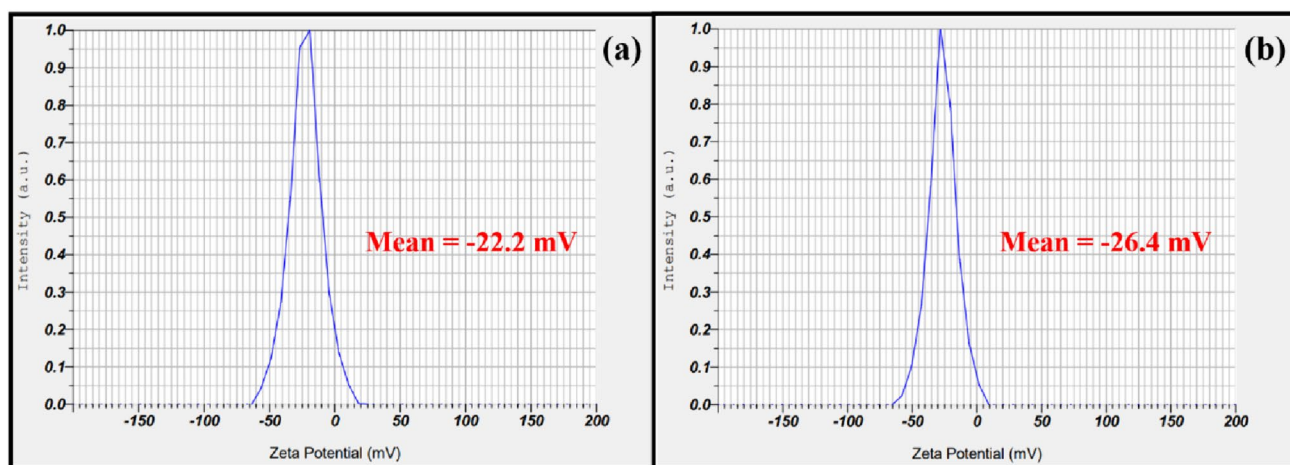


Fig. 6 Zeta potential analysis of **a** ZnFe_2O_4 NPs **b** ZnF: GO nanocomposites

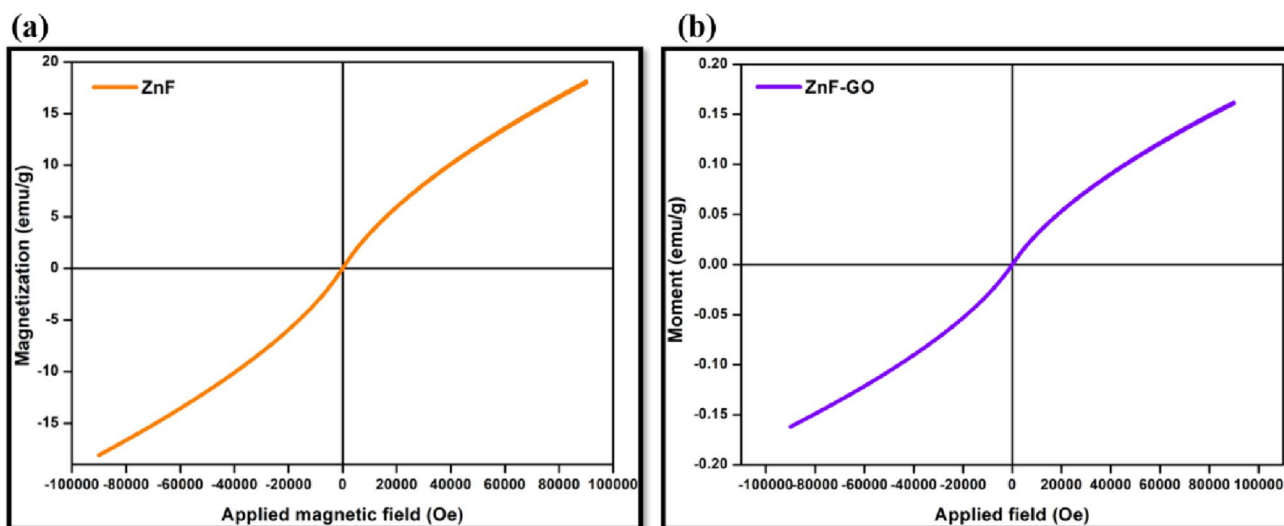


Fig. 7 Hysteresis curve @ 300 K for a $ZnFe_2O_4$ and b $ZnFe_2O_4/GO$ nanocomposites

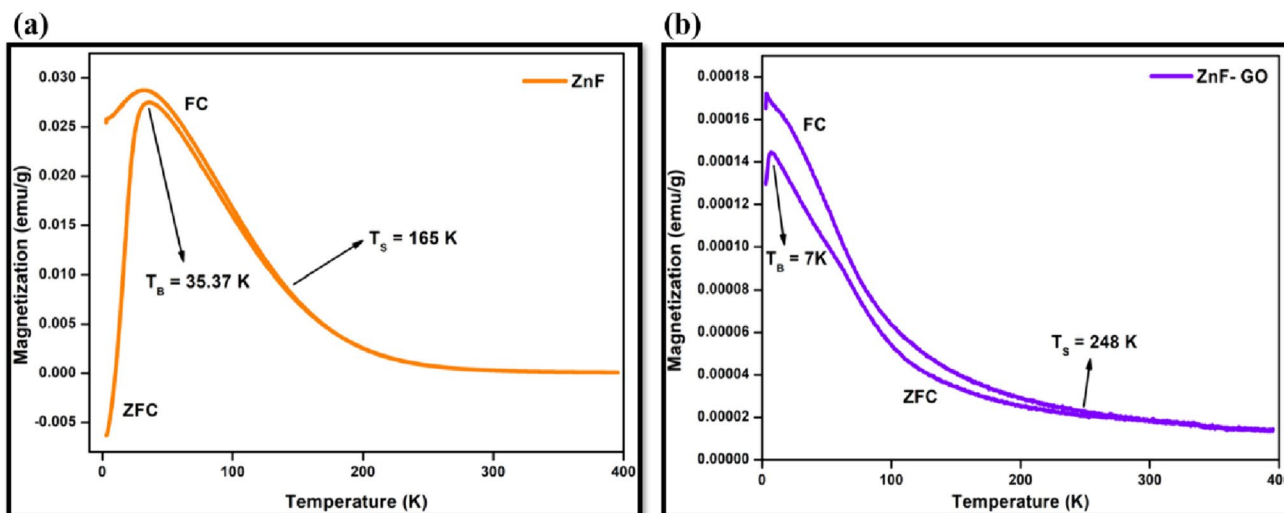


Fig. 8 ZFC and FC curves from 0 to 400 K for a $ZnFe_2O_4$ and b $ZnFe_2O_4/GO$ nanocomposites

ZnF and ZnF/GO nanoparticles from the maximum magnetization of ZFC and FC curves, and it is said to be the blocking temperatures, respectively. The narrow distribution of particles in zinc ferrites is caused by the difference between T_B and T_S . The hysteresis curves of zinc ferrite/GO nanocomposites are observed to be devoid of magnetic saturation.

The presence of transition metal constituents enhances the role of relativistic effects (spin–orbit coupling) upon diverse material properties. The magnetic anisotropy within mixed spinel nano ferrites like ZFO is hence the consequence of spin polarization effects and partial quenching of angular momentum. This causes an increase in the degree of anisotropy and the subsequent accommodation of electrons in the Fe-3d orbitals (Silva et al. 2019). However, a

contrasting impact with GO-doped composition is the aftermath of disproportionate carbon and oxygen distributions alongside the removal of a few oxygen atoms within the coupled composition. As a result, increasing occupancy of non-magnetic material constituents within GO-doped compositions weakens the resultant magnetic response of the material. In compliance with the electrophysical essence, the magnetic behavior of spinel nano ferrites with key insights can be elaborately understood with the associated magnetic parameters. ZFO-based mixed spinel nano ferrites are thus a class of materials the former desirable prerequisites. Table 6 below indicates the magnetic moment and the resultant saturation magnetization of pure and GO-doped ZFO compositions as a function of the degree of inversion (x).

Table 6 DFT simulated magnetic property of pure and GO-doped ZFO compositions

Composition	DFT simulated magnetic parameters		
	Degree of inversion (x)	Magnetic moment (μ_B) (emu/g)	Saturation magnetization (M_s) (emu/g)
ZFO	0	3.604	83.486
	0.15	3.618	83.810
	0.25	3.624	83.949
	0.35	3.546	82.142
	0.45	3.511	81.332
	0.55	3.405	78.876
	0.65	3.335	77.255
GO-ZFO	0	2.765	64.051
	0.15	2.823	65.394
	0.25	2.881	66.738
	0.35	2.752	63.749
	0.45	2.701	62.568
	0.55	2.625	60.807
	0.65	2.534	58.699

A superparamagnetic response is recorded for the pure ZFO composition due to the mixed spinel structure while a decreasing attribute is obtained with GO-doped composition due to the non-magnetic nature of graphene oxide. DFT simulated saturation magnetization ($M_s = 83.949$ emu/g) of mixed spinel ZFO from Table 6 goes in agreement with our experimental outcomes and the works of (Noreen et al. 2022) respectively. However, the strength of the net magnetization of such mixed spinel nano ferrites is purely non-linear which relies heavily upon the inversion parameter ‘ x ’ in the skeletal formula unit. The inversion parameter is thus responsible for the cationic migrations and the net magnetic moment of the overall composition.

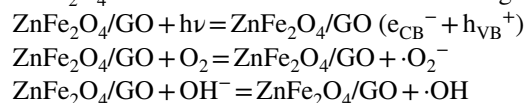
The non-linear behavior of M_s with respect to the inversion parameter is the consequence of structural entropy which increases up to a threshold and decreases thereafter due to magnetic phase transitions. The saturation magnetization gradually increases with a consequent rise in ‘ x ’ ($x \leq 0.25$) due to preserved structural integrity. Besides, prominent contributions to the magnetic behavior of the overall composition originate from the A-site Zn^{2+} cations in $(Zn_{1-x}Fe_x)[Zn_xFe_{2-x}]$, respectively. However, a subsequent hike in the degree of inversion ($x > 0.25$) causes a successive replacement of Zn^{2+} cations with Fe^{3+} cations at the tetrahedral site. A significantly large inversion parameter ($x \sim 1$) spoils the structural integrity with a complete Fe^{3+} tetrahedral occupancy and causes a division of the B-site into multiple sub-lattices with a consequent rotation of the magnetic dipole. As a result, the tetrahedral-occupied Fe^{3+} cations no longer favor the ferrimagnetic arrangements of

magnetic moments relative to Fe^{2+} cations in the octahedral interstice. In compliance with the statistical results shown in Table 6, a congruent trend is obtained with GO-doped compositions.

The origin of transit in the magnetic response of dual composition is observed beyond $x > 0.5$. The consequent attribute is due to the overpopulation of non-magnetic Zn and GO in the octahedral sites of the resultant compositions leads to the proportional distributions of magnetic cations in the tetrahedral and octahedral interstices which nullifies the net magnetic moment (Bohra et al. 2021). Besides, a steep decline in the saturation magnetization ($M_s = 66.738$ emu/g corresponding to $x = 0.25$) of GO-doped hybrid ($\sim 20.5\%$ with respect to ZFO) is due to a predominant paramagnetic response with rising GO concentrations in the overall composition. Meanwhile, Go-doped ZFO also demonstrates a high resistance to magnetic field line penetrations due to the heterostructure magneto dielectric interface that may induce partial diamagnetic behavior (Ali et al. 2022). As a result, pure ZFO mixed spinel nano ferrites with a low degree of inversion are a potential candidate for water reclamation applications.

Photocatalytic analysis

Figure 9 displays UV–Vis–NIR absorption spectra of zinc ferrite nanocomposites, which illustrates their photocatalytic potential. When exposed to visible light, the samples of zinc ferrite/GO nanocomposites with organic pollutants (MB dyes) absorb the light, which causes the electrons in the valence band to move into the conduction band, where they form an electron–hole pair on the surface of the catalyst (Thandapani et al. 2018; Cheng et al. 2004). Conduction band electrons (e_{CB}^-) and oxygen molecules interact to produce superoxide radicals. Additionally, OH^- is converted to $\cdot OH$ (hydroxyl radical) via the existing holes in the valence band (Dutta et al. 2024; Patial et al. 2023). In general, the photocatalytic function of nanocomposites consisting of organic components is represented by following equations. ZnF and ZnF/GO nanocomposites have been found to have the degradation efficiencies of 60 and 85.8%, respectively. The existence of graphene oxide in zinc ferrite nanoparticles increases the efficiency of degradation of organic pollutants like methylene blue dye. The primary benefits of implementing MB are its affordable price and accessibility (Ghazkoob et al. 2022; Gul et al. 2020). The degradation test was carried over an irradiation time of 60 min. Further, Photo-Fenton reaction can be initiated by Fe^{3+} on the surface of $ZnFe_2O_4$ to form $OH\cdot$ radicals in the following ways,



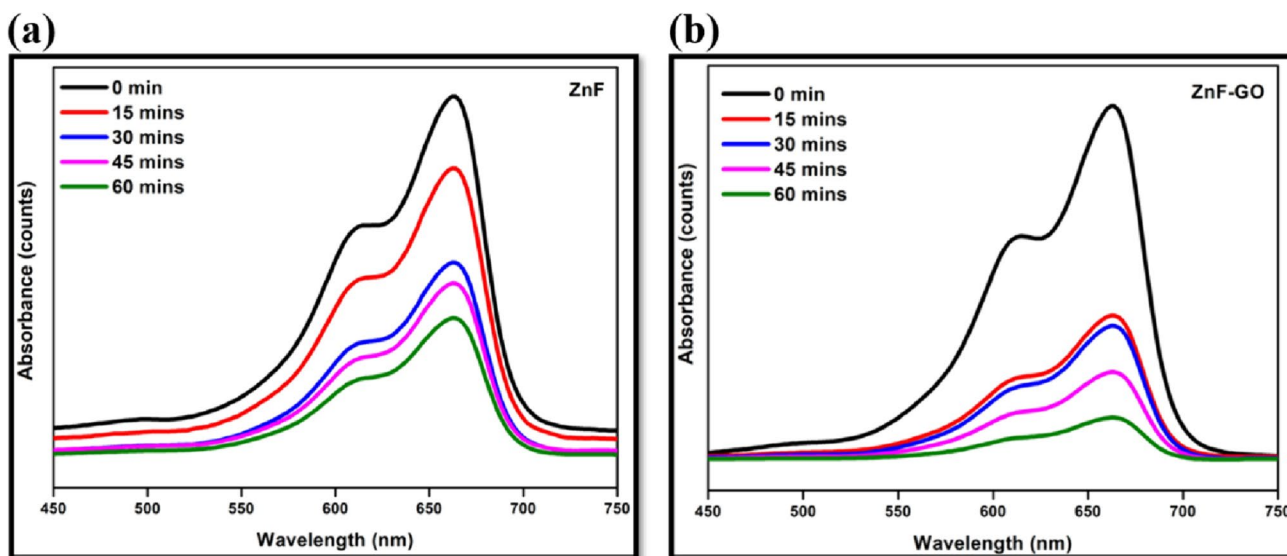


Fig. 9 UV (degradation) spectra of ZnFe₂O₄: GO nanocomposites

Hydrogen peroxide (H₂O₂) + hν (visible light) = ·OH + OH⁻

Hydrogen peroxide + e_{CB}⁻ = ·OH + OH⁻

Fe³⁺ + hydrogen peroxide = Fe²⁺ + ·HO₂ + H⁺

Fe²⁺ + hydrogen peroxide = Fe³⁺ + ·OH + OH⁻

H₂O + h_{VB}⁺ = ·OH + H⁺

Hydrogen peroxide + h_{VB}⁺ = ·O₂⁻ + 2H⁺

ZnFe₂O₄/GO + ·OH + ·O₂⁻ + organic dye (methylene blue) = ZnFe₂O₄/GO + H₂O + CO₂

In addition, a pseudo first-order kinetic model was fitted to examine the linear performance of the deterioration

performance; the resulting data are displayed in Fig. 10b. The pseudo first-order kinetic model fits all the samples well. The photocatalyst was extracted from each cycle, washed, and left to dry overnight at 60 °C. Figure 11b illustrates the outstanding photostability and durability of the obtained nanocomposite, which were determined by XRD analysis based on the recycling process (Yang et al. 2017). Also, it ensures that there are no extra peaks in the pattern by displaying both new and used ZnF–GO photocatalyst for the first and fifth cycles of degradation. It is

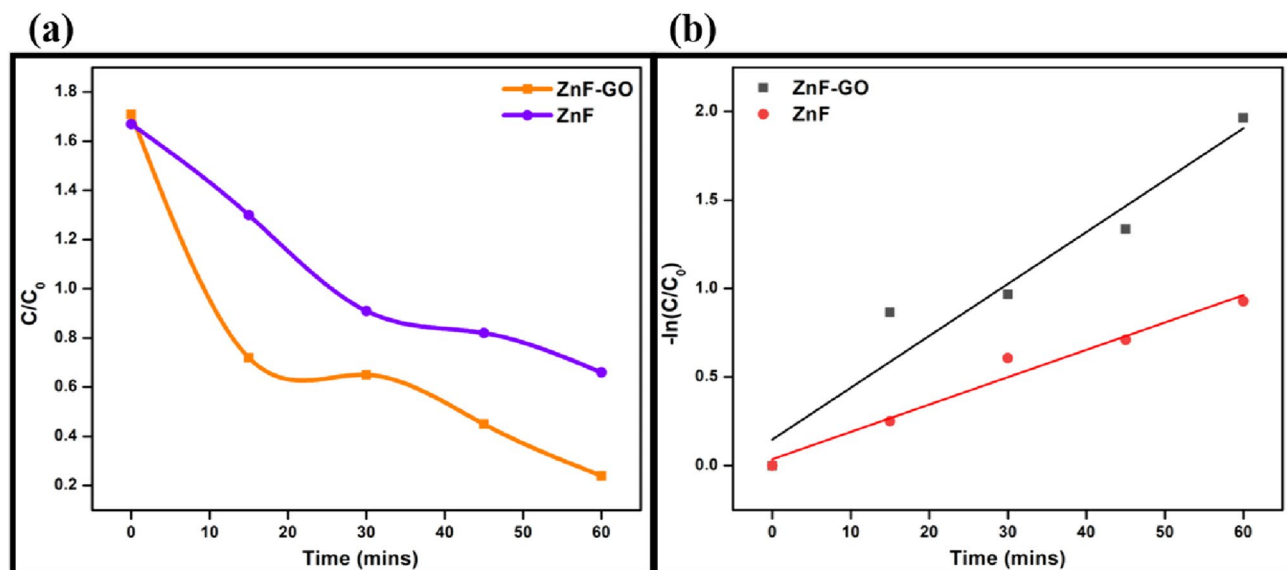


Fig. 10 a Photocatalytic degradation of methylene blue dye and b pseudo first-order kinetic model of ZnF–GO nanocomposite

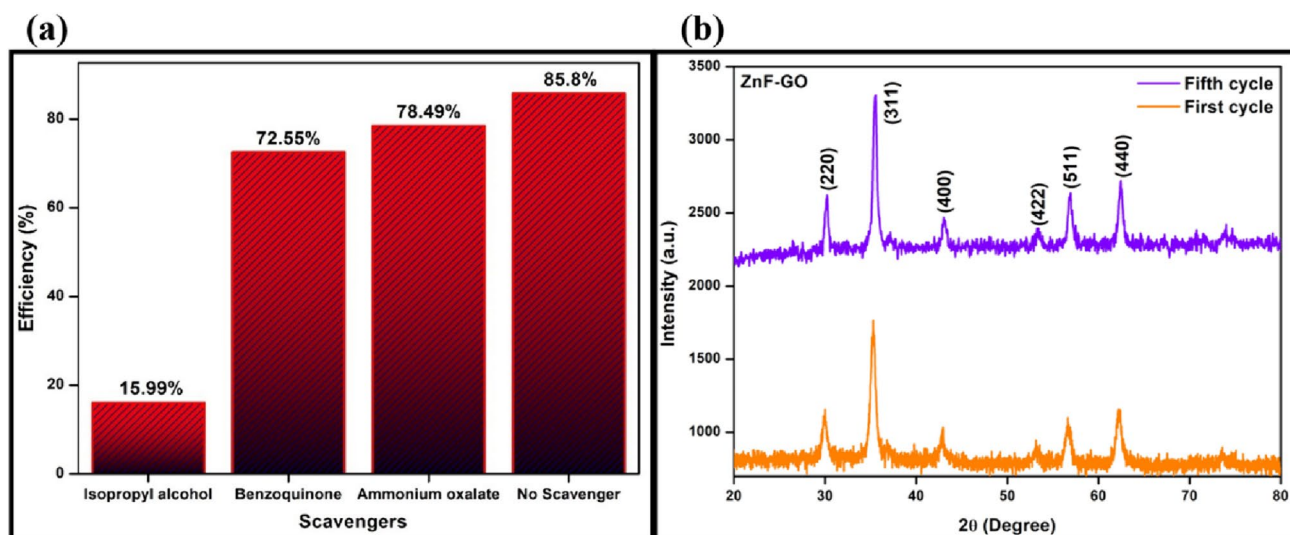


Fig. 11 **a** Catalytic performance of methylene blue dye with various scavengers in the presence of ZnF-GO photocatalyst and **b** XRD patterns of ZnF-GO nanocomposite for first and fifth cycles of the degradation process

thus shown by XRD analysis that the produced ZnF-GO photocatalyst was extremely stable.

The reactive species that are active in the photocatalytic system can be identified by a scavenger test. Several radical species, including isopropyl alcohol, benzoquinone, and ammonium oxalate, were employed to investigate how different active species, like superoxide, holes, and hydroxyl radicals, influence photocatalytic degradation. Just a negligibly tiny percentage of the degradation process was lowered by adding ammonium oxalate and benzoquinone to the dye solution, as shown in Fig. 11a. It demonstrates unequivocally that superoxide radicals and holes have very little effect on the deterioration process (Palanisamy et al. 2024). Furthermore, after adding isopropyl alcohol scavenger to the catalytic reactor, the hydroxyl radical degradation efficiency dropped from 85.8% to 15.99%. Thus, it is evident that hydroxyl radicals are important to the photocatalytic breakdown of methylene blue dye. Based on the aforementioned outcomes, the ZnF-GO nanocomposite catalyst system has effectively assisted in the hydroxyl radical's breakdown of the methylene blue dye process. The energy bandgap figures from the UV analysis make it abundantly evident that the photocatalyst components can absorb visible light. As a result, our optical analysis of the ZnFe₂O₄/GO nanocomposites indicates towards their superior suitability for employment in photocatalysis for the preservation of the environment.

Conclusion

The co-precipitation approach yielded ZnFe₂O₄/GO nanocomposites with good structural, morphological, optical, and magnetic measurements, making them appropriate for photocatalytic applications. A larger crystalline size and lower band gap values are characteristics of a high-quality photocatalyst compound. Also, the correlation between the structure and optical features shown in both experimental and theoretical analysis reveal that the prepared nanocomposite can function as a good photocatalyst rather than in magnetic storage applications. Moreover, the samples exhibit superparamagnetic behaviour at ambient temperature during paramagnetic ordering in the magnetic domain. According to theoretical part, Go-doped ZnF demonstrates a strong resistance to magnetic field line penetrations due to the heterostructure magneto dielectric interface which may induce partial diamagnetic behavior. Thus, the optical properties of the synthesized nanoferrites proved them to be a good material for the purpose of photocatalyst and could degrade the organic based compounds like methylene blue present in the drinking water.

Data availability Data will be made available on the request.

Declaration

Conflict of interest The authors have no conflicts of interest.

References

- Ahmed MA, Ahmed MA, Mohamed AA (2022) Facile adsorptive removal of dyes and heavy metals from wastewaters using magnetic nanocomposite of zinc ferrite@reduced graphene oxide. *Inorg Chem Commun* 144:109912. <https://doi.org/10.1016/j.inoche.2022.109912>
- Ait Kerroum MA, Essyed A, Iacovita C, Baaziz W, Ihiwakrim D, Mounkachi O, Hamedoun M, Benyoussef A, Benaissa M, Ersen O (2019) The effect of basic pH on the elaboration of ZnFe₂O₄ nanoparticles by co-precipitation method: structural, magnetic and hyperthermia characterization. *J Magn Magn Mater* 478:239–246. <https://doi.org/10.1016/j.jmmm.2019.01.081>
- Ajormal F, Moradnia F, Taghavi Fardood S, Ramazani A (2020) Zinc ferrite nanoparticles in photo-degradation of dye: mini-review. *J Chem Rev* 2:90–102. <https://doi.org/10.33945/sami/jcr.2020.2.2>
- Ali R, Aziz MH, Gao S, Khan MI, Li F, Batool T, Shaheen F, Qiu B (2022) Graphene oxide/zinc ferrite nanocomposite loaded with doxorubicin as a potential theranostic medium in cancer therapy and magnetic resonance imaging. *Ceram Int* 48:10741–10750. <https://doi.org/10.1016/j.ceramint.2021.12.290>
- Andjelković L, Šuljagić M, Lakić M, Jeremić D, Vulić P, Nikolić AS (2018) A study of the structural and morphological properties of Ni–ferrite, Zn–ferrite and Ni–Zn–ferrites functionalized with starch. *Ceram Int* 44:14163–14168. <https://doi.org/10.1016/j.ceramint.2018.05.018>
- Baynosa ML, Mady AH, Nguyen VQ, Kumar DR, Sayed MS, Tuma D, Shim JJ (2020) Eco-friendly synthesis of recyclable mesoporous zinc ferrite@reduced graphene oxide nanocomposite for efficient photocatalytic dye degradation under solar radiation. *J Colloid Interface Sci* 561:459–469. <https://doi.org/10.1016/j.jcis.2019.11.018>
- Bhuvaneshwari K, Palanisamy G, Bharathi G, Pazhanivel T, Upadhyaya IR, Kumari MLA, Rajesh RP, Govindasamy M, Ghfar A, Al-Shaalan NH (2021) Visible light driven reduced graphene oxide supported ZnMgAl LTH/ZnO/g-C₃N₄ nanohybrid photocatalyst with notable two-dimension formation for enhanced photocatalytic activity towards organic dye degradation. *Environ Res*. <https://doi.org/10.1016/j.envres.2021.111079>
- Bibi F, Ahmed A, Ajaj Y, Dawood AAAS, Usman M, Alodhayb A, Mohammad S, Ahmad Z, Kalsoom A, Iqbal S (2024) Fabrication of Ni and Mn co-doped ZnFe₂O₄ spinel ferrites and their nanocomposites with rGO as an efficient photocatalyst for the remediation of organic dyes. *Polyhedron* 250:116826. <https://doi.org/10.1016/j.poly.2024.116826>
- Bohra M, Alman V, Arras R (2021) Nanostructured znfe₂o₄: an exotic energy material. *Nanomaterials* 11:1–24. <https://doi.org/10.3390/nano11051286>
- Chen J, Yao B, Li C, Shi G (2013) An improved Hummers method for eco-friendly synthesis of graphene oxide. *Carbon* 64:225–229
- Cheng P, Li W, Zhou T, Jin Y, Gu M (2004) Physical and photocatalytic properties of zinc ferrite doped titania under visible light irradiation. *J Photochem Photobiol A Chem* 168:97–101. <https://doi.org/10.1016/j.jphotochem.2004.05.018>
- da Silva FG, Depuyrot J, Campos AFC, Aquino R, Fiorani D, Peddis D (2019) Structural and magnetic properties of spinel ferrite nanoparticles. *J Nanosci Nanotechnol* 19:4888–4902. <https://doi.org/10.1166/jnn.2019.16877>
- Dippong T, Levei EA, Cadar O (2021) Formation, structure and magnetic properties of mfe₂o₄@sio₂ (M = co, mn, zn, ni, cu) nanocomposites. *Materials (basel)* 14:1–15. <https://doi.org/10.3390/ma14051139>
- Dudarev S, Botton G (1998) Electron-energy-loss spectra and the structural stability of nickel oxide: An LSDA+U study. *Phys Rev B—condens Matter Mater Phys* 57:1505–1509. <https://doi.org/10.1103/PhysRevB.57.1505>
- Dutta V, Sonu, Sudhaik A, Kumar R, Raizada P, Ahamad T, Alshehri SM, Thakur S, Van Le Q, Kaya S, Hu C, Nguyen VH, P. (2024) Singh, emergence of S-scheme-derived Ag decorated CuBi₂O₄/CNTs/(BiO)₂CO₃ photocatalyst with enhanced visible light photocatalytic performance. *J Taiwan Inst Chem Eng*. <https://doi.org/10.1016/j.jtice.2023.105319>
- Džunuzović AS, Ilić NI, Vijatović Petrović MM, Bobić JD, Stojadinović B, Dohčević-Mitrović Z, Stojanović BD (2015) Structure and properties of Ni–Zn ferrite obtained by auto-combustion method. *J Magn Magn Mater* 374:245–251. <https://doi.org/10.1016/j.jmmm.2014.08.047>
- Farhang M, Ghadiri AM, Hassani P, Akbarzadeh AR (2024) Highly efficient ZnFe₂O₄ decorated g-C₃N₄/GO with biomedical and photocatalytic activities. *Ceram Int*. <https://doi.org/10.1016/j.ceramint.2024.01.076>
- Fei P, Wang Q, Zhong M, Su B (2016) Preparation and adsorption properties of enhanced magnetic zinc ferrite-reduced graphene oxide nanocomposites via a facile one-pot solvothermal method. *J Alloys Compd* 685:411–417. <https://doi.org/10.1016/j.jallcom.2016.05.279>
- Fei L, Ali F, Said A, Tariq N, Raziq F, Ali N, Arif U, Akhter MS, Rahdar A, Bilal M (2023) Surface-functionalized spongy zinc ferrite as a robust visible-light driven nanocatalyst for wastewater remediation: characterization, kinetic, and mechanistic insight. *Int J Environ Sci Technol* 20:1007–1018. <https://doi.org/10.1007/s13762-022-04026-w>
- Fesenko O, Yatsenko L (2017) Nanophysics, Nanomaterials, Interface Studies, and Applications. Springer Proceedings in Physics, 195
- Garza-Tovar L, Torres-Martinez L, Bernal Rodriguez D, Gomez R, Del Angel G (2006) Photocatalytic degradation of methylene blue on Bi. *J Mol Catal A Chem* 247:283–290. <https://doi.org/10.1007/s10854-023-10866-0>
- Gaur DK, Pandey FP, Rastogi A, Parmar AS, Manohar R, Singh S (2022) Investigation of dielectric, optical and zeta potential properties of pure and zinc ferrite nanoparticles dispersed nematic liquid crystal PCH5. *Appl Phys A Mater Sci Process* 128:1–11. <https://doi.org/10.1007/s00339-022-05318-1>
- Gharagozlou M, Bayati R (2015) Low temperature processing and magnetic properties of zinc ferrite nanoparticles. *Superlattices Microstruct* 78:190–200. <https://doi.org/10.1016/j.spmi.2014.12.004>
- Ghazkoob N, Zargar Shoushtari M, Kazeminezhad I, Lari Baghal SM (2022) Investigation of structural, magnetic, optical and photocatalytic properties of zinc ferrite nanowires/bismuth vanadate composite. *J Alloys Compd* 900:163467. <https://doi.org/10.1016/j.jallcom.2021.163467>
- Grasset F, Labhsetwar N, Li D, Park DC, Saito N, Haneda H, Cadore O, Roisnel T, Mornet S, Duguet E, Portier J, Etourneau J (2002) Synthesis and magnetic characterization of zinc ferrite nanoparticles with different environments: powder, colloidal solution, and zinc ferrite-silica core-shell nanoparticles. *Langmuir* 18:8209–8216. <https://doi.org/10.1021/la020322b>
- Gul S, Yousuf MA, Anwar A, Warsi MF, Agboola PO, Shakir I, Shahid M (2020) Al-substituted zinc spinel ferrite nanoparticles: preparation and evaluation of structural, electrical, magnetic and photocatalytic properties. *Ceram Int* 46:14195–14205. <https://doi.org/10.1016/j.ceramint.2020.02.228>

- Guo X, Zhu H, Li Q (2014) Visible-light-driven photocatalytic properties of ZnO/ZnFe₂O₄ core/shell nanocable arrays. *Appl Catal B Environ* 160–161:408–414. <https://doi.org/10.1016/j.apcatb.2014.05.047>
- Hangai B, Borsari E, Aguiar EC, Garcia FG, Longo E, Simões AZ (2017) Superparamagnetic behaviour of zinc ferrite obtained by the microwave assisted method. *J Mater Sci Mater Electron* 28:10772–10779. <https://doi.org/10.1007/s10854-017-6854-1>
- Jalili H, Aslibeiki B, Hajalilou A, Musalu O, Ferreira LP, Cruz MM (2022) Bimagnetic hard/soft and soft/hard ferrite nanocomposites: structural, magnetic and hyperthermia properties. *Ceram Int* 48:4886–4896. <https://doi.org/10.1016/j.ceramint.2021.11.025>
- Kmita A, Lachowicz D, Zukrowski J, Gajewska M, Szczerba W, Kuciakowski J, Zapotoczny S, Sikora M (2019) One-step synthesis of long term stable superparamagnetic colloid of zinc ferrite nanorods in water. *Materials (basel)*. <https://doi.org/10.3390/ma12071048>
- Latif S, Liaqat A, Imran M, Javaid A, Hussain N, Jesionowski T, Bilal M (2023) Development of zinc ferrite nanoparticles with enhanced photocatalytic performance for remediation of environmentally toxic pharmaceutical waste diclofenac sodium from wastewater. *Environ Res* 216:114500. <https://doi.org/10.1016/j.envres.2022.114500>
- Liu X, Pan L, Zhao Q, Lv T, Zhu G, Chen T, Lu T, Sun Z, Sun C (2012) UV-assisted photocatalytic synthesis of ZnO-reduced graphene oxide composites with enhanced photocatalytic activity in reduction of Cr(VI). *Chem Eng J* 183:238–243. <https://doi.org/10.1016/j.cej.2011.12.068>
- Mahmood M, Yousuf MA, Baig MM, Imran M, Suleman M, Shahid M, Khan MA, Warsi MF (2018) Spinel ferrite magnetic nanostructures at the surface of graphene sheets for visible light photocatalysis applications. *Phys B Condens Matter* 550:317–323. <https://doi.org/10.1016/j.physb.2018.08.043>
- Nandhini G, Vignesh D, Shobana MK (2023) Structural and optical integrity of pure and NiFe₂O₄-GO nanoferrite: a combined experimental and first principles approach. *Inorg Chem Commun* 158:111662. <https://doi.org/10.1016/j.inoche.2023.111662>
- Noreen S, Hussain A, Tahir MB, Ziya AB, Rehman JU, Usman M, Khan SA, Akhtar S (2022) Structural, mechanical, thermodynamic, electronic, magnetic and optical properties of ZnFe₂O₄ ferrite: a DFT study. *Opt Mater (amst)* 133:112930. <https://doi.org/10.1016/j.optmat.2022.112930>
- Palanisamy G, Bhuvanewari K, Lee J, Viji A, Shkir M (2024) Strategic rationalization for improved photocatalytic decomposition of toxic pollutants: immobilizing Bi₂Te₃ nanorods and V₂O₅ nanoparticles over MoS₂ nanosheets. *Spectrochim. Acta—part A Mol Biomol Spectrosc* 304:123400. <https://doi.org/10.1016/j.saa.2023.123400>
- Parasuraman B, Shanmugam P, Govindasamy P, Nangan S, Gnana-sekaran L, Thangavelu P (2023) Photocatalytic degradation of tetracycline contaminated wastewater over Bi₂S₃/BiWO₆/rGO ternary nanocomposite under visible light irradiation. *J Taiwan Inst Chem Eng*. <https://doi.org/10.1016/j.jtice.2023.105249>
- Patial S, Sonu, Sudhaik A, Chandel N, Ahamad T, Raizada P, Singh P, Chaukura N, Selvasembian R (2022) A review on carbon quantum dots modified g-C₃N₄-based photocatalysts and potential application in wastewater treatment. *Appl Sci*. <https://doi.org/10.3390/app122111286>
- Patial S, Sonu, Thakur S, Van Le Q, Ahamad T, Singh P, Nguyen VH, Khan AAP, Hussain CM, Raizada P (2023) Facile synthesis of Co, Fe-bimetallic MIL-88A/microcrystalline cellulose composites for efficient adsorptive and photo-Fenton degradation of RhB dye. *J Taiwan Inst Chem Eng* 153:105189. <https://doi.org/10.1016/j.jtice.2023.105189>
- Patil BA, Kounsalye JS, Humbe AV, Kokate RD (2021) Structural, magnetic, dielectric and hyperfine interaction studies of titanium (Ti⁴⁺)-substituted nickel ferrite (Ni_{1-x}Ti_xFe_{2-2x}O₄) nanoparticles. *J Mater Sci Mater Electron* 32:4556–4567. <https://doi.org/10.1007/s10854-020-05197-3>
- Pham PV, Bodepudi SC, Shehzad K, Liu Y, Xu Y, Yu B, Duan X (2022) 2D heterostructures for ubiquitous electronics and optoelectronics: principles, opportunities, and challenges. *Chem Rev* 122:6514–6613. <https://doi.org/10.1021/acs.chemrev.1c00735>
- Qadir A, Le TK, Malik M, Amedome Min-Dianey KA, Saeed I, Yu Y, Choi JR, Pham PV (2021) Representative 2D-material-based nanocomposites and their emerging applications: a review. *RSC Adv* 11:23860–23880. <https://doi.org/10.1039/d1ra03425a>
- Rachna NB, Singh A (2018) Agarwal, preparation, characterization, properties and applications of nano zinc ferrite. *Mater Today Proc* 5:9148–9155. <https://doi.org/10.1016/j.matpr.2017.10.035>
- Sari RS, Hakim AR (2019) Bonding analysis of magnetic nanoparticles (MNPS) zinc ferrite (ZnFe₂O₄) encapsulated with silica (SiO₂). *IOP Conf Ser Earth Environ Sci*. <https://doi.org/10.1088/1755-1315/382/1/012019>
- Shobana MK, Nandhini G, Kavita S, Suresh Kumar V, Pazhanivel T (2022) Photocatalytic and magnetic properties of Mg substituted cobalt ferrite. *Mater Sci Eng B Solid-State Mater Adv Technol* 286:116030. <https://doi.org/10.1016/j.mseb.2022.116030>
- Sonu V, Dutta A, Sudhaik AAP, Khan T, Ahamad P, Raizada S, Thakur AM, Asiri P (2023) Singh, GCN/CuFe₂O₄/SiO₂ photocatalyst for photo-Fenton assisted degradation of organic dyes. *Mater Res Bull* 164:112238. <https://doi.org/10.1016/j.materresbull.2023.112238>
- Sudha D, Sivakumar P (2015) Review on the photocatalytic activity of various composite catalysts. *Chem Eng Process Process Intensif* 97:112–133. <https://doi.org/10.1016/j.cep.2015.08.006>
- Sutka A, Millers M, Vanags M, Joost U, Maiorov M, Kisand V, Pärna R, Juhnevica I (2015) Comparison of photocatalytic activity for different co-precipitated spinel ferrites. *Res Chem Intermed* 41:9439–9449. <https://doi.org/10.1007/s11164-015-1969-6>
- Szotek Z, Temmerman WM, Ködderitzsch D, Svane A, Petit L, Winter H (2006) Electronic structures of normal and inverse spinel ferrites from first principles. *Phys Rev B - Condens Matter Mater Phys* 74:1–12. <https://doi.org/10.1103/PhysRevB.74.174431>
- Thandapani P, Ramalinga Viswanathan M, Denardin JC (2018) Magnetocaloric effect and universal curve behavior in superparamagnetic zinc ferrite nanoparticles synthesized via microwave assisted co-precipitation method. *Phys Status Solidi Appl Mater Sci*. <https://doi.org/10.1002/pssa.201700842>
- Vinoshia PA, Mely LA, Jeronsia JE, Krishnan S, Das SJ (2017) Synthesis and properties of spinel ZnFe₂O₄ nanoparticles by facile co-precipitation route. *Optik (stuttg)* 134:99–108. <https://doi.org/10.1016/j.ijleo.2017.01.018>
- Yang C, Qin J, Xue Z, Ma M, Zhang X, Liu R (2017) Rational design of carbon-doped TiO₂ modified g-C₃N₄ via in-situ heat treatment for drastically improved photocatalytic hydrogen with excellent photostability. *Nano Energy* 41:1–9. <https://doi.org/10.1016/j.nanoen.2017.09.012>

Publisher's Note Springer Nature remains neutral with regard to jurisdictional claims in published maps and institutional affiliations.

Springer Nature or its licensor (e.g. a society or other partner) holds exclusive rights to this article under a publishing agreement with the author(s) or other rightsholder(s); author self-archiving of the accepted manuscript version of this article is solely governed by the terms of such publishing agreement and applicable law.